A Lagrangian stochastic model of surf zone drifter dispersion

Matthew S. Spydell[1] and Falk Feddersen[1]

Received 21 October 2011; revised 5 January 2012; accepted 7 February 2012; published 29 March 2012.

[1] Drifter-derived cross-shore and alongshore surf zone diffusivities were previously estimated on an alongshore uniform beach over 1000 s for five Huntington Beach, California, 2006 (HB06) experiment release days. The cross-shore diffusivity K_x had a nonmonotonic time dependence, potentially due to the shoreline or to weaker diffusivity seaward of the surf zone. The alongshore diffusivities K_y were qualitatively consistent with shear dispersion but differed from the classic Taylor laminar theory. Here, modeled and analytic diffusivities for the five release days are derived from a Lagrangian stochastic model (LSM) that uses the drifter-derived bulk (cross-shore averaged) velocity variance and cross-shore-dependent mean alongshore current. The LSM modeled and analytic cross-shore diffusivities are nonmonotonic due to the shoreline and strongly suggest that the observed cross-shore diffusivity is shoreline affected. The LSM typically reproduce well the observed K_x with Lagrangian time scale between 75 and 200 s, consistent with surf zone eddy time scales. HB06 drifter trajectories were too short to observe the analytic long-time K_x limit, and weaker diffusivity seaward of the surf zone may be important at longer times (>1000 s). On all release days, the LSM model and analytic alongshore diffusivity reproduce well the observed K_y with alongshore Lagrangian time scales between 95 and 155 s. The isolated shear-induced diffusivity is very well represented by an analytic theory which incorporates a nonzero Lagrangian time scale. Many of the stochastic model parameters can be specified a priori with reasonable assumptions to predict surf zone dispersion of an initial value problem pollution spill.

Citation: Spydell, M. S., and F. Feddersen (2012), A Lagrangian stochastic model of surf zone drifter dispersion, *J. Geophys. Res.*, *117*, C03041, doi:10.1029/2011JC007701.

1. Introduction

[2] Elevated levels of surf zone contaminants, whether fecal indicator bacteria [*Reeves et al.*, 2004] or viruses [*Jiang and Chu*, 2004], increase health risks to ocean bathers [*Haile et al.*, 1999] and lead to beach closures [*Boehm et al.*, 2002]. The surf zone is also habitat to ecologically important species of fish, invertebrates, and macroalgae [e.g., *Brown and McLachlan*, 2002]. Understanding tracer transport and diffusion (dilution) is critical for predicting beach water quality or for larval recruitment. For a known surf zone source, tracer (pollution, larvae, etc.) transport up or down coast is understood for simple relatively alongshore uniform beaches [*Ruessink et al.*, 2001; *Grant et al.*, 2005]. However, surf zone diffusion, which impacts the fate of surf zone fecal indicator bacteria (M. Rippy et al., Factors controlling patchiness in nearshore fecal pollution— Part 1: Fecal indicator bacteria as passive particles, manuscript in preparation, 2011), is not as well understood.

[3] Surf zone drifters have been used both experimentally [*Spydell et al.*, 2007, 2009; *Brown et al.*, 2009] and numerically [*Spydell and Feddersen*, 2009; *Geiman et al.*, 2011] to estimate cross-shore and alongshore surf zone absolute diffusivities and to investigate the mechanisms driving drifter dispersion. Similarly, surf zone dye observations [*Clark et al.*, 2010] and numerical simulations [*Clark et al.*, 2011] have also been used to estimate surf zone tracer dispersion and its mechanisms. For times greater than a few wave periods, drifter and dye cross-shore dispersion is due to low-frequency (<0.03 Hz) surf zone eddies [*Spydell and Feddersen*, 2009; *Clark et al.*, 2010, 2011].

[4] Lagrangian-derived diffusivities are time dependent. In homogeneous turbulence, the diffusivity K is monotonic with a linear ballistic regime ($K = \overline{u^2}t$, where t is time and $\overline{u^2}$ is the velocity variance) for times much less than the Lagrangian time scale τ and become constant ($K = \overline{u^2}\tau$) at times much larger than τ [*Taylor*, 1922]. For five drifter release days on an alongshore uniform beach, the cross-shore (x) and alongshore (y) diffusivities (K_x and K_y, respectively) were estimated for times less than 1000 s using an unbiased estimator [*Spydell et al.*, 2009].

[5] The observed K_x had a ballistic regime for $t < 50$ s, a K_x maximum ≈ 2 m^2 s^{-1} around 150–300 s, with slow decay for longer times (Figure 1a). The time to reach maximum and the long-time decay rate varied with release day. This nonmonotonic K_x pattern was not generally observed by *Spydell et al.* [2007] on another alongshore uniform beach

[1]Integrative Oceanography Division, Scripps Institution of Oceanography, University of California, San Diego, La Jolla, California, USA.

0148-0227/12/2011JC007701

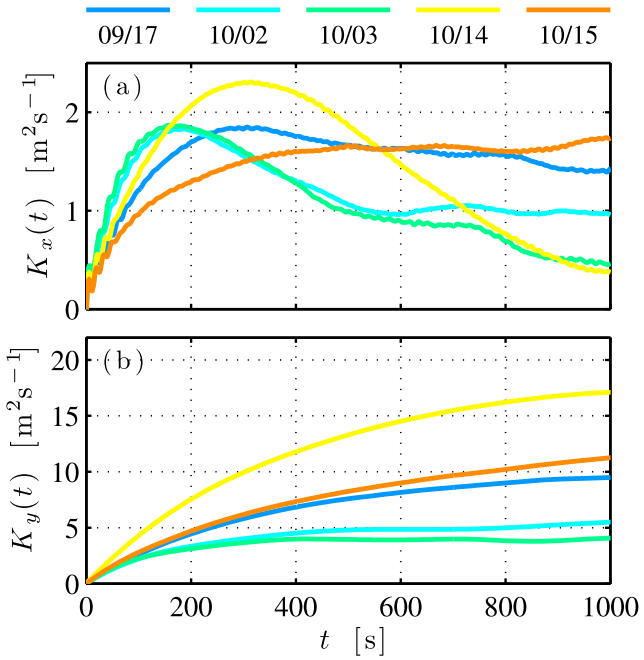

Figure 1. The drifter-derived observed (a) cross-shore K_x and (b) alongshore K_y diffusivity versus time on the five HB06 release days given by the legend [from *Spydell et al.*, 2009].

because biased estimators were used. On a rip-channeled beach, nonmonotonic K_x time dependence also was observed [*Brown et al.*, 2009], although this was linked to the transit time through the rip circulation cells.

[6] A nonmonotonic surf zone K_x may occur either because the shoreline boundary prevents unbounded diffusion or because diffusion is weaker seaward of the surf zone. Consistent with weaker seaward of the surf zone diffusivity, observed and modeled low-frequency rotational velocities (eddy energy) are significantly weaker just 60 m seaward of the surf zone [*Feddersen et al.*, 2011]. At short times, both *Spydell et al.* [2007] and *Brown et al.* [2009] found K_x weaker seaward of the surf zone relative to within the surf zone. However at longer times, larger sampling errors and biases prevent determining if K_x was smaller seaward of the surf zone. *Brown et al.* [2009] observed that very few drifters left the surf zone during their deployments, suggesting weak diffusion offshore. Similarly, *Spydell et al.* [2009] also found that surf zone-released drifters rarely went more than 60 m offshore of the surf zone during 10–20 min releases. *Reniers et al.* [2009] found that including low-frequency eddies was crucial to reproducing the observed [*Brown et al.*, 2009] surf zone drifter ejection statistics.

[7] The observed alongshore diffusivity K_y, for the Huntington Beach, California, 2006 experiment (HB06) drifters [*Spydell et al.*, 2009], is larger than K_x and grows monotonically (Figure 1b). The ramp-up time scales are large (>340 s) for three release days, and for the 1000 s of observations, the observed K_y did not always asymptote [*Spydell et al.*, 2009]. The inferred long-time alongshore diffusivity K_y was proportional to the maximum alongshore current squared, qualitatively consistent with the *Taylor* [1953] theory of laminar shear dispersion in a pipe, but differing by a factor of 3. However, the *Taylor* [1953] theory, which effectively assumes a zero Lagrangian time scale, may not be applicable in the surf zone where the Lagrangian time scale (i.e., time-correlated Lagrangian velocities) is nonzero owing to finite-sized horizontal eddies [*Spydell and Feddersen*, 2012]. The relative contribution of eddy-induced (random) dispersion and shear dispersion on the surf zone alongshore diffusivity is not known.

[8] Modeled surf zone drifter diffusivities (and other statistics) can be derived from numerical drifters seeded into wave-resolving Boussinesq models [*Spydell and Feddersen*, 2009; *Geiman et al.*, 2011] or wave-averaged circulation models [*Reniers et al.*, 2009]. In these models, a rich wave number spectrum of rotational (eddies) velocities advect numerical drifters [e.g., *Spydell and Feddersen*, 2009], which can complicate diagnosing the causes of the observed time-dependent K_x and K_y behavior.

[9] A simpler approach is to simulate Lagrangian particle trajectories (similar to a random walk) with a Lagrangian stochastic model (LSM) using Langevin equations to represent particle position and velocity. LSMs have been used extensively to study dispersion in homogeneous turbulence [e.g., *Rodean*, 1996], two-dimensional turbulence [*Pasquero et al.*, 2001], the atmospheric boundary layer [*Wilson and Sawford*, 1996], basin-scale oceanic dispersion [*Berloff and McWilliams*, 2002], coastal oceanography [*Brickman and Smith*, 2002], and the dispersion of coastal larvae [*Siegel et al.*, 2003]. For some applications the LSM can be solved analytically [*Wilson et al.*, 2003] leading to precise time-dependent diffusivities.

[10] Here, using mean current, bulk velocity variance, and Lagrangian time scale as input, a LSM that includes a shoreline boundary is used to investigate the features of the HB06 observed cross-shore (K_x) and alongshore (K_y) diffusivities (Figure 1). The HB06 drifter observations and the diffusivity estimation methods are described in section 2. Langevin equations are presented section 3.1, and some analytic solutions to them are given in section 3.2. Section 3.3 explains how the HB06 drifter data and statistics are modeled using the LSM. The modeled and analytic cross-shore diffusivity K_x are shown to reproduce the time-dependent observed $K_x(t)$ (section 4.1) and suggests that the nonmonotonic observed diffusivity is due to shoreline effects. Also, the modeled and observed alongshore diffusivities $K_y(t)$ agree very well (section 4.2). The isolated modeled and observed shear-induced diffusivity agree very well with the analytic shear dispersion solution that includes a nonzero Lagrangian time scale [*Spydell and Feddersen*, 2012]. On the release days with stronger alongshore currents (and shear), shear dispersion is the dominant contribution to $K_y(t)$. The results, assumptions, and implications are discussed in section 5. In particular, without a priori knowledge of the model input parameters, guidance is provided for parameterizing these quantities for predicting the evolution of the initial value problem of a surf zone contaminant spill (section 5.3). The results are summarized in section 6.

2. HB06 Drifter Observations

[11] Surf zone drifter release experiments were performed near Huntington Beach, California, as part of the Fall 2006 HB06 experiment [*Spydell et al.*, 2009]. Relevant details of

Table 1. Incident Significant Wave Height H_s, Maximum Alongshore Current V_m, and Surf Zone Width L_{sz} on the Five Drifter Release Days as Reported by *Spydell et al.* [2009]

	17 Sep	2 Oct	3 Oct	14 Oct	15 Oct
H_s (m)	0.83	0.68	0.65	0.69	0.68
V_m (m s^{-1})	0.27	–0.13	–0.17	0.35	0.25
L_{sz} (m)	99	74	79	79	79

the experiments are briefly described here. The cross-shore coordinate x increases negatively offshore ($x = 0$ m is at the mean shoreline) and the alongshore coordinate y increases upcoast. The bathymetry was approximately alongshore uniform. Ten, 50 cm tall, surf zone GPS-tracked drifters, that track cross-shore and alongshore positions ($x(t)$, $y(t)$) at 1 Hz [*Schmidt et al.*, 2003], were deployed on five release days (17 September and 2, 3, 14, and 15 October 2006) with variable incident wave and mean current conditions (Table 1). Using values of *Spydell et al.* [2009], the surf zone width L_{sz} was generally between 75 and 100 m from the shoreline (Table 1). Drifters were released repeatedly within or near the surf zone, and allowed to drift freely for 15–30 min before being collected and rereleased. Drifter tracks suggest advection by alongshore currents and the presence of low-frequency ($f < 0.03$ Hz) eddies. Drifters rarely advected more than 160 m offshore from the shoreline. Due to their finite depth, some GPS-tracked drifters were beached at the shoreline and needed to be rereleased farther offshore. In such cases, the drifter track was terminated at the shoreline (i.e., absorbing the drifter) and the drifter was rereleased in deeper water. On the other hand, some drifters were not completely beached and "reflected" off of the shoreline. Thus, the shoreline boundary condition for the observed drifters is mixed, partially absorbing and partially reflecting.

[12] As the irrotational (sea swell band) surface gravity wave motions are not directly responsible for surf zone dispersion [*Spydell and Feddersen*, 2009], the drifter positions are wave averaged using a Gaussian filter with a low-pass cutoff of 0.033 Hz. From these low-pass drifter positions, drifter velocity time series $(\dot{x}(t), \dot{y}(t))$ are calculated as finite differences, i.e.,

$$\dot{x}(t) = \frac{x(t+\Delta t) - x(t)}{\Delta t}, \qquad (1)$$

where t is time and Δt is the sampling interval.

[13] For each release, the cross-shore drifter position probability distribution function (pdf) $p(x)$, the drifter-derived quasi-Eulerian mean alongshore current $V(x)$, and velocity variances ($\overline{u^2}(x)$ and $\overline{v^2}(x)$) are estimated in 16–25 m wide (depending on release day) cross-shore bins. The averaging is over all times and drifters within a bin. The velocity variances are considered quasi-Eulerian as binned Lagrangian statistics can differ from Eulerian ones [e.g., *Davis*, 1991]. However, the cross-shore structure of these drifter-derived binned velocity statistics are similar to velocity statistics observed from a cross-shore array of acoustic Doppler velocimeters (ADV) [*Spydell et al.*, 2009].

[14] The drifter cross-shore position pdf $p(x)$ was nonuniform across the surf zone with a maximum generally within the surf zone (Figure 2a), indicating that drifters were more likely to sample the midsurf zone than seaward of the surf zone ($x < -100$ m) or near the shoreline ($x \approx 0$ m). Three drifter release days (17 September, 14 October, and 15 October) had strong positive mean alongshore currents $V(x)$ with maximum velocity between 0.3 and 0.6 m s^{-1} and were significantly sheared (Figure 2b). In contrast, two release days (2 and 3 October) had negative and weak $V(x)$ (≈ -0.2 m s^{-1}) with limited velocity shear (Figure 2b). On each day the cross-shore velocity variance $\overline{u^2}$ has a maximum around 0.02–0.04 m^2 s^{-2} in the midsurf zone ($x \approx -50$ m in Figure 2c). The alongshore velocity variance $\overline{v^2}$ has similar magnitude to the cross-shore ones (Figure 2d), with typically less cross-shore structure than $\overline{u^2}$ and a maximum generally at or closer to the shoreline. The cross-shore structure of the low-frequency Lagrangian velocity variances are consistent with the Eulerian low-frequency velocity variances observed on different days [*Feddersen et al.*, 2011].

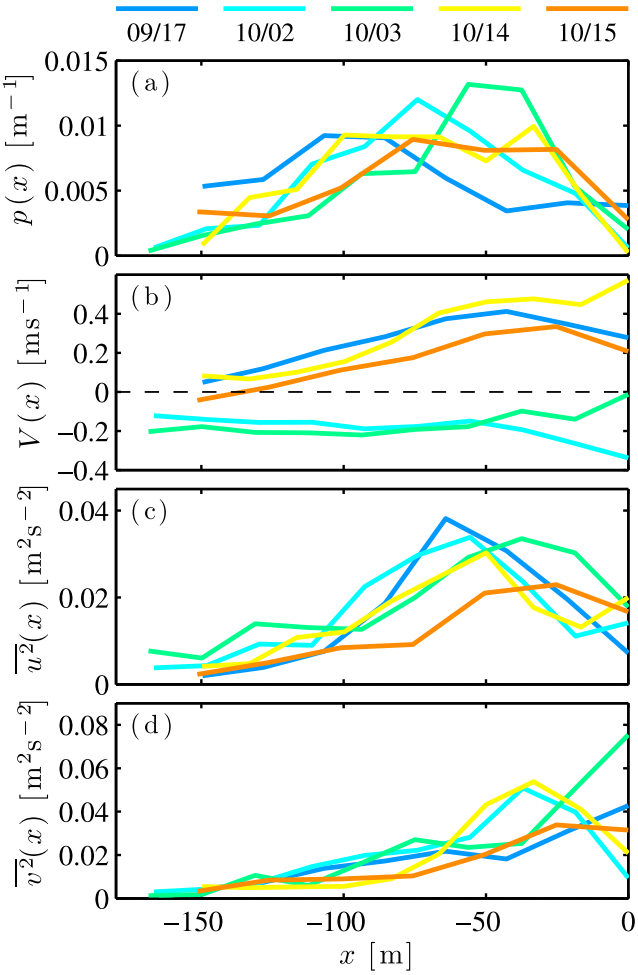

Figure 2. Binned drifter statistics versus the cross-shore coordinate x on each of the five HB06 release days (colors): (a) the probability distribution function of cross-shore drifter position $p(x)$, (b) mean alongshore current $V(x)$, (c) low-frequency ($f < 0.03$ Hz) cross-shore $\overline{u^2}(x)$ and (d) alongshore $\overline{v^2}(x)$ drifter velocity variances. Cross-shore bin width varies between 16 and 25 m, and the cross-shore extent of Lagrangian observations varies between 150 and 169 m, depending on the day.

[15] Following *Spydell et al.* [2009], drifter-derived diffusivities are estimated using the unbiased Lagrangian velocity autocovariance, defined for cross-shore velocities as $C_x(t)$,

$$C_x(t) = \langle \dot{x}(a+t)\dot{x}(a)\rangle - \langle \dot{x}(a+t)\rangle\langle \dot{x}(a)\rangle, \tag{2}$$

where angle brackets represent an average over all available time lags t on a trajectory and an average over all trajectories. Averaging over all possible time lags t on a trajectory, i.e., averaging over a, assumes that a trajectory's velocity is stationary. On the HB06 drifter release days, the cross-shore ($K_x(t)$) and alongshore ($K_y(t)$) diffusivities (Figure 1) are estimated from the time integral of the Lagrangian velocity autocovariance function [i.e., *Taylor*, 1922]

$$K_x(t) = \int_0^t C_x(t')\mathrm{d}t'. \tag{3}$$

Although surf zone statistics are inhomogeneous and depend on cross-shore position, the diffusivity is calculated as if the statistics were homogeneous, hence K_x and K_y are "bulk" quantities which average over all the various cross-shore-dependent motions.

3. The Lagrangian Stochastic Model

[16] In this section, the Lagrangian stochastic model (LSM) is introduced. In section 3.1, the Langevin equations for particle motion are stated. In order to gain some perspective into the properties and statistics of the LSM, analytic solutions to the Langevin equations are presented in section 3.2. Section 3.3 explains how the observed HB06 drifter data are simulated using the LSM.

3.1. The Langevin Equations

[17] Particle trajectories are modeled using the Langevin equations for particle velocity and position,

$$\frac{\mathrm{d}u}{\mathrm{d}t} = -\frac{u}{\tau_x} + \sqrt{\frac{2\sigma_u^2}{\tau_x}}w_x, \tag{4a}$$

$$\frac{\mathrm{d}v}{\mathrm{d}t} = -\frac{v}{\tau_y} + \sqrt{\frac{2\sigma_v^2}{\tau_y}}w_y, \tag{4b}$$

$$\frac{\mathrm{d}x}{\mathrm{d}t} = u, \tag{4c}$$

$$\frac{\mathrm{d}y}{\mathrm{d}t} = V(x) + v, \tag{4d}$$

where (x, y) refers to the particle position. Two-dimensional particle motion is considered because the drifter observations are two-dimensional. In addition, the surf zone is a shallow water fluid with depth (<3 m) much less than the horizontal scales (>10 m) of dispersion, and where strong breaking-wave-generated turbulence [e.g., *Feddersen*, 2012] leads to strong vertical mixing. Furthermore, two-dimensional models of tracer dispersion can explain observed surf zone cross-shore dye tracer dispersion. [*Clark et al.*, 2010, 2011]. The particle's random cross-shore and alongshore velocities are u and v, respectively, with variances denoted by σ_u^2 and σ_v^2. Particle velocities are correlated in time with the memory of prior velocity over the specified Lagrangian time scale $\tau_{x,y}$. Although inhomogeneous Lagrangian velocity variance and time scales can be included [e.g., *Wilson and Sawford*, 1996], for simplicity, cross-shore homogeneous (spatially uniform) statistics are considered here. The cross-shore sheared mean alongshore current $V(x)$ in (4d) advects particles. The cross-shore mean Lagrangian current (the sum of onshore Stokes drift and offshore Eulerian return flow) must be zero to prevent accumulation of mass at the shoreline.

[18] Thus, the model (4) can be thought of as representing depth integrated Lagrangian motions for which the cross-shore mean Lagrangian velocity is zero. The $w_{x,\ y}(t)$ are zero mean, stationary, white noise processes with variance (squared ensemble average) $\langle w_i(t)w_j(t')\rangle = \delta(t - t')\delta_{ij}$ so that $\int_0^t w_i(t')dt'$ are independent, incremental Weiner processes. Although the shoreline boundary condition for the observed drifters is mixed (due to terminating the trajectories of beached drifters), the model shoreline at $x = 0$ reflects particles resulting in a zero particle flux through the shoreline. The reflecting boundary condition is chosen as it is the appropriate boundary condition for tracer (dye, pollution) dispersion. Moreover, the results which follow are not significantly sensitive to the particular shoreline boundary condition (absorbing, reflecting, or mixed).

[19] For $\tau_x = \tau_y = 0$, the set of four Langevin equations (4) reduces to two equations for the (x, y) position with noise added directly to the positions [e.g., *Zambianchi and Griffa*, 1994], resulting in a classical Brownian random walk. The cross-shore equations (4a) and (4c) do not depend on the alongshore variables (y, v), thus cross-shore Lagrangian statistics are independent of the alongshore. On the other hand, alongshore Lagrangian statistics depend upon cross-shore Lagrangian model parameters due to $V(x)$.

3.2. LSM Analytic Solutions

[20] Here, the ensemble-averaged analytic diffusivity is derived from the Langevin equations (4) for three situations. (1) Concepts and terminology are briefly introduced and reviewed for an unbounded (infinite) domain. (2) Then a semi-infinite domain corresponding to shoreline-bounded cross-shore surf zone drifter dispersion is considered. (3) Alongshore shear dispersion driven by cross-shore variable alongshore current $V(x)$ is considered. In contrast to the averaging over all available time lags on a trajectory and over trajectories used in (2), analytic diffusivities K(a) are derived using (ensemble) averages, represented here by angle brackets, which only average over trajectories.

3.2.1. Unbounded (Infinite) Domain

[21] In an infinite domain without a mean current, the ensemble average statistics of (4a) and (4c) are well known [see *Uhlenbeck and Ornstein*, 1930], and detailed derivations are omitted. Denoting a drifter trajectory as $x(t|x_0)$ with initial position x_0, i.e., $x(t = 0) = x_0$, and assuming a random initial velocity with mean square value σ_u^2, the ensemble mean position is

$$\overline{X}(t|x_0) \equiv \langle x(t|x_0)\rangle = x_0$$

and the ensemble mean squared position is

$$\overline{X^2}(t|x_0) \equiv \left\langle [x(t|x_0)]^2 \right\rangle = x_0^2 + 2\sigma_u^2\tau_x\left[t + \tau_x e^{-t/\tau_x} - \tau_x\right]. \quad (5)$$

As positions are Gaussian [*Uhlenbeck and Ornstein*, 1930], the drifter positions pdf $P(x, t|x_0)$ at time t, for a particle released at x_0, is given by

$$P(x,t|x_0) = \frac{1}{\sqrt{2\pi\sigma_x^2(t)}}\exp\left[-\frac{(x-x_0)^2}{2\sigma_x^2(t)}\right], \quad (6)$$

where the drifter displacement variance is defined as

$$\sigma_x^2(t) \equiv \overline{X^2}(t|x_0) - \left[\overline{X}(t|x_0)\right]^2 = 2\kappa_x\left[t + \tau_x e^{-t/\tau_x} - \tau_x\right], \quad (7)$$

and $\kappa_x \equiv \sigma_u^2\tau_x$ is the long-time diffusivity. The bulk diffusivity $K_x(t|x_0)$ is half the time derivative of the drifter displacement variance,

$$K_x(t|x_0) \equiv \frac{1}{2}\frac{d}{dt}\sigma_x^2(t) = \kappa_x\left(1 - e^{-t/\tau_x}\right), \quad (8)$$

recovering the classic ballistic ($K_x \approx \sigma_u^2 t$ for $t \ll \tau_x$) and Brownian ($K_x \approx \kappa_x$, for $t \gg \tau_x$) dispersion regimes [*Taylor*, 1922].

3.2.2. Bounded (Semi-infinite) Domain

[22] Here, the cross-shore diffusivity is derived for drifters released at x_0 ($x_0 < 0$) on a semi-infinite domain with a reflecting boundary at $x = 0$ and no mean cross-shore currents. This is considered the "half-line problem." As the shoreline boundary reflects drifters, the boundary condition at $x = 0$ is no flux and the half-line (denoted by a subscript H) problem drifter position pdf $P_H(x, t, |x_0)$ is, using the method of images,

$$P_H(x,t|x_0) = P(x,t|x_0) + P(x,t|-x_0), \quad (9)$$

where $P(x, t|x_0)$ is the infinite domain drifter position pdf (6). The half-line mean drifter position is

$$\overline{X}_H(t|x_0) = \int_{-\infty}^{0} x P_H(x,t|x_0)\,dx \quad (10)$$

and performing the integral (10) gives a time-dependent mean position $\overline{X}_H(t|x_0)$ for the half-line problem,

$$\overline{X}_H(t|x_0) = -\sqrt{\frac{2}{\pi}}\sigma_x \exp\left[-\frac{x_0^2}{2\sigma_x^2(t)}\right] - x_0 \mathrm{erf}\left[\frac{x_0}{2^{1/2}\sigma_x(t)}\right], \quad (11)$$

where $\sigma_x^2(t)$ is given by (7). The half-line mean position (11) monotonically decreases with time as particles, unable to cross the shoreline, must eventually move negatively offshore.

[23] The time when the shoreline is encountered, t_0, occurs when $\sigma_x^2(t_0) = x_0^2$. Defining the nondimensional distance to the shoreline as

$$\alpha = \frac{x_0^2}{\kappa_x\tau_x}, \quad (12)$$

the time t_0 is given by

$$t_0/\tau_x = \begin{cases} \alpha^{1/2} & \text{for } \alpha \ll 1 \\ \alpha/2 & \text{for } \alpha \gg 1. \end{cases} \quad (13)$$

These cases correspond to whether dispersion is ballistic (first case, $\sigma_x^2 = \sigma_u^2 t^2$) or Brownian (second case, $\sigma_x^2 = 2\kappa t$) when the boundary is encountered. For $t \ll t_0$ the mean drifter position is the release location and $\overline{X}_H(t) \approx x_0$. For $t \gg t_0$ the mean drifter position is given by

$$\overline{X}_H(t|x_0) \approx -\sqrt{\frac{2}{\pi}}\sigma_x(t). \quad (14)$$

[24] The "half-line" mean square position

$$\overline{X_H^2} = x_0^2 + \sigma_x^2$$

is identical to that for the unbounded domain, but due to the mean position $\overline{X}_H(t|x_0)$ time dependence, the half-line bulk diffusivity $K_x^{(a)}(t|x_0)$

$$\begin{aligned} K_x^{(a)}(t|x_0) &= \frac{1}{2}\frac{d}{dt}\overline{X_H^2}(t|x_0) - \overline{X}_H(t|x_0)\frac{d}{dt}\overline{X}_H(t|x_0) \\ &= \kappa_x\left(1 - e^{-t/\tau_x}\right) - \overline{X}_H(t|x_0)\frac{d}{dt}\overline{X}_H(t|x_0), \end{aligned} \quad (15)$$

differs from the unbounded domain case. Plugging (11) into (15) yields

$$\begin{aligned} K_x^{(a)}(t|x_0) = \kappa_x &\left[1 - e^{-t/\tau_x}\right] \\ &\cdot \left[1 - \frac{2}{\pi}e^{-\alpha/2t''} - \sqrt{\frac{\alpha}{\pi t''}}e^{-\alpha/4t''}\mathrm{erf}\left(\sqrt{\frac{\alpha}{4t''}}\right)\right], \end{aligned} \quad (16)$$

where

$$t'' = t/\tau_x + e^{-t/\tau_x} - 1.$$

[25] The presence of the shoreline boundary can significantly effect the bulk diffusivity. The half-line $K_x^{(a)}$ (16) is always less than that for the unbounded case (8). For drifters released at $x_0 = 0$, the boundary is instantly felt, and the bulk diffusivity is $K_x^{(a)} = \kappa_x(1 - 2/\pi)[1 - \exp(-t/\tau_x)]$ (see $\alpha = 0.001$ curve in Figure 3). For $x_0 \neq 0$ and $t \ll t_0$ the bulk diffusivity $K_x^{(a)} \approx \kappa_x[1 - \exp(-t/\tau_x)]$ tracks that for the infinite domain (see $\alpha = 10^3$ curve for $t/\tau_x < 10^2$ in Figure 3). For $\alpha = 10^3$ and for $t \gg t_0$, the bulk diffusivity tracks the half-line bulk diffusivity for particles released from $x_0 = 0$. The transition between these unbounded domain and shoreline release behaviors occurs when $t \approx t_0$ resulting in a distinct diffusivity maxima for some α (see $\alpha = 10$ curve in Figure 3). For all α, when $t \gg t_0$, the long-time bulk diffusivity is reduced by a factor of $(1 - 2/\pi)$ relative to the unbounded domain K_x.

[26] For any pdf of initial release locations $p_0(x_0)$, the mean drifter location is calculated via,

$$\overline{X}_H(t|p_0) = \int_{-\infty}^{0} p_0(x_0)\overline{X}_H(t|x_0)\,dx_0,$$

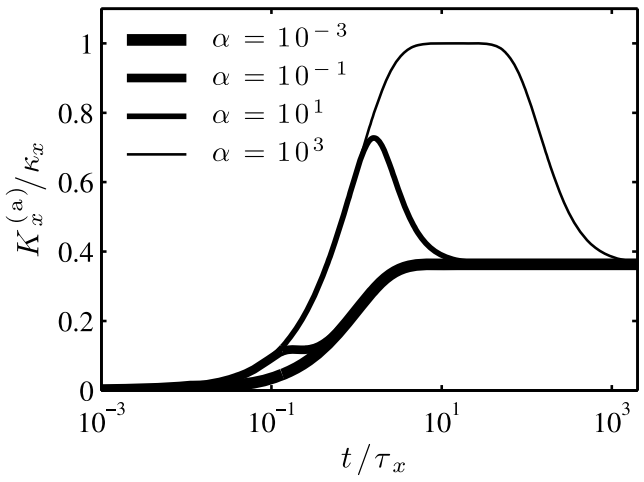

Figure 3. The analytic half-line nondimensional diffusivity $K_x^{(a)}/\kappa_x$ versus nondimensional time t/τ_x (16). Line thickness indicates various nondimensional release location $\alpha = x_0^2/(\kappa_x\tau_x)$ (see legend).

where $\overline{X}_H(t|x_0)$ is given by (11). Note that $p_0(x_0)$ is distinct from the pdf of all cross-shore positions $p(x)$ (Figure 2a). Regardless of the initial release location pdf $p_0(x_0)$, the mean squared drifter position contribution to the diffusivity is $\kappa_x(1 - e^{-t/\tau_x})$. Therefore, the analytic diffusivity for any $p_0(x_0)$ is $K_x^{(a)}(t|p_0)$ and given by (15) with $\overline{X}_H(t|p_0)$ instead of $\overline{X}_H(t|x_0)$. The analytic cross-shore diffusivity $K_x^{(a)}$ will be compared to observed diffusivities in section 4.1.

3.2.3. Alongshore Shear Dispersion

[27] Here, analytic expressions for the alongshore drifter diffusivity induced by the sheared mean alongshore current $V(x)$ (i.e., shear dispersion) are presented. The theory of shear dispersion, first developed for laminar pipe flows [*Taylor*, 1953], was extended by *Spydell and Feddersen* [2012] to include the effect of nonzero cross-shore Lagrangian time scale τ_x. The alongshore diffusivity can be written as

$$K_y(t) = \kappa_y\left(1 - e^{-t/\tau_y}\right) + K_S(t), \tag{17}$$

where the first term on the right-hand side of (17) is the contribution of random alongshore particle motions due to surf zone eddies and the second term K_S is the shear-induced diffusivity. For an alongshore current $V(x)$ over cross-shore extent L_V, with Fourier cosine coefficients

$$V_n = \frac{2}{L_V}\int_0^{L_V} \cos(n\pi x/L_V)V(x)\mathrm{d}x,$$

the analytic shear-induced bulk alongshore diffusivity $K_S^{(a)}$ for cross-shore uniformly released drifters is [*Spydell and Feddersen*, 2012]

$$K_S^{(a)}(t) = \sum_{n=1}^{\infty} \frac{V_n^2}{2}\int_0^t e^{-\frac{1}{2}\left(\frac{n\pi}{L_V}\right)^2 \sigma_x^2(t')}\mathrm{d}t', \tag{18}$$

where $\sigma_x^2(t') = 2\kappa_x(t' + \tau_x e^{-t'/\tau_x} - \tau_x)$. The shear dispersion contribution to the observed alongshore diffusivity is analyzed using (18) in section 4.2.

3.3. LSM Simulations of HB06 Data

[28] In addition to comparing observed diffusivities to analytic ones, the HB06 drifter data set is stochastically reproduced using the LSM. For each day, modeled drifter trajectories are computed by numerically integrating the Langevin equations (4) using specified model parameters. A realization of modeled trajectories is obtained using the identical trajectory number, initial position (release location) and trajectory length, and with Gaussian random initial velocity. From the simulated trajectories, modeled diffusivities $K(\mathrm{m})_{x,y}$ are calculated via (3) similar to the observed $K(\mathrm{o})_{x,y}$.

[29] Unlike the analytic diffusivity solutions which are exact for a set of model parameters, the sampling error for diffusivity derived from trajectories (either observed or modeled) depends on the number of trajectories. For a single realization of a days worth of drifter observations, the observed diffusivity sampling error (ϵ_{K_x}) can be significant [*Spydell et al.*, 2009]. The diffusivity (or other moments) sampling error is approximately inversely proportional to the square root of the number of drifters, thus the model diffusivity sampling error can be reduced to some predetermined threshold by increasing the number of simulated drifters. Here, ten times the number of observed drifters (10 realizations) are used in the model, reducing the modeled diffusivity sampling error ($\approx \epsilon_{K_x}/\sqrt{10}$).

[30] For each day, the observed binned $V(x)$ (Figure 2b, where the cross-shore bins are 16–25 m wide depending on the day), with offshore $V(x) = 0$ (at $x = -1000$ m) is linearly interpolated to the drifter cross-shore position for use in the model. Although the cross-shore and alongshore drifter velocity variances vary in the cross-shore (Figures 2c

Table 2. Various Cross-Shore Diffusivity K_x LSM Parameters for the Five HB06 Drifter Release Days[a]

	17 Sep	2 Oct	3 Oct	14 Oct	15 Oct
σ_u^2 ($m^2\ s^{-2}$)	0.017	0.023	0.025	0.018	0.014
τ_x (s)	125(±30)	75(±20)	75(±15)	125(±35)	200(±70)
$K_x^{(m)}$ ($K_x^{(a)}$) RMSE ($m^2\ s^{-1}$)	0.06 (0.37)	0.22 (0.15)	0.25 (0.22)	0.55 (0.55)	0.16 (0.42)
$K_x^{(m)}$ ($K_x^{(a)}$) skill	0.99 (0.94)	0.97 (0.98)	0.95 (0.96)	0.87 (0.87)	0.99 (0.91)
$\overline{x_0}$ (m)	−73	−71	−58	−55	−38
α	20	40	23	11	3

[a]The model (analytic) K_x root-mean-square error (RMSE) is defined as the $\langle(K_x^{(m)} - K_x^{(o)})^2\rangle^{1/2}$, and skill is defined as $1 - \mathrm{RMSE}^2/\langle(K_x^{(o)})^2\rangle$, where angle brackets denote a 1000 s time average. The analytic $K_x^{(a)}$ RMSE and skill are shown in parentheses. The τ_x error bars are defined as the τ_x change that increases the RMSE by $0.2[\langle(K_x^{(o)})^2\rangle]^{1/2}$. The $\overline{x_0}$ is the average over all release locations (open circles in Figure 4) and α (12) is estimated with $\overline{x_0}$.

Table 3. Alongshore Diffusivity K_y LSM Model Parameters and Skills for the Five HB06 Drifter Release Days[a]

	17 Sep	2 Oct	3 Oct	14 Oct	15 Oct
σ_v^2 (m^2 s^{-2})	0.020	0.027	0.028	0.025	0.020
τ_y (s)	95(±65)	140(±50)	100(±30)	105(±80)	155(±65)
$K_y^{(m)}$ RMSE (m^2 s^{-1})	0.43	0.13	0.21	1.02	0.30
$K_y^{(m)}$ skill	0.99	0.99	0.99	0.99	0.99

[a]The K_y RMSE and skill and the τ_y error bars are defined as in Table 2.

and 2d), for simplicity bulk (scalar) cross-shore (σ_u^2) and alongshore (σ_v^2) velocity variances are used as model input. The σ_u^2 and σ_v^2 are calculated as the weighted (by drifter cross-shore position $p(x)$, Figure 2a) surf zone average of the observed cross-shore-dependent $\overline{u^2}(x)$ and $\overline{v^2}(x)$ (Figures 2c and 2d), i.e., for σ_u^2,

$$\sigma_u^2 = \int_{x=-160\mathrm{m}}^{x=0\mathrm{m}} \overline{u^2}(x)p(x)\mathrm{d}x. \tag{19}$$

Over the five release days, the bulk σ_u^2 varies between 0.014 and 0.025 m^2 s^{-2} (Table 2) and σ_v^2 varies between 0.020 and 0.028 m^2 s^{-2} (Table 3).

[31] Unlike drifter velocity variances, the spatially constant cross-shore (τ_x) and alongshore (τ_y) Lagrangian time scales cannot be a priori derived from the drifter observations without invoking additional assumptions. In the open ocean, the Lagrangian time scale is typically between 0.5 and 1.25 times the Eulerian time scale [*Lumpkin et al.*, 2002] and is consistent with the *Middleton* [1985] formula. Lagrangian time scales smaller than Eulerian time scales are expected for eddies that are relatively strong, small, and persistent. Although the precise relationship between Lagrangian and Eulerian time scales is unknown in the surf zone, as the horizontal eddies responsible for dispersion have significant energy in the Eulerian time scales of 33–250 s [*Feddersen et al.*, 2011], τ_x and τ_y are expected to fall within this range. Within this $\tau_{x,y}$ range, modeled and observed drifter trajectories are qualitatively similar (Figure 4).

[32] The modeled diffusivities $K_x^{(m)}(t)$ depend on τ_x (Figure 5). For example, on release day 17 September, the modeled $K_x^{(m)}$ (i.e., the mean of the diffusivities found for the 10 realizations of modeled 17 September drifter tracks) with τ_x = 125 s is very similar to the observed diffusivity $K_x^{(o)}$ over the entire 1000 s of observations (compare solid and dashed curves in Figure 5). The uncertainty in the modeled diffusivity is small and is approximately $\sim \pm\epsilon_{K_x}/10^{1/2}$ (ϵ_{K_x} is the gray shading in Figure 5). For smaller τ_x = 50 s, $K_x^{(m)}$ deviates significantly from the observed $K_x^{(o)}$ by ramping up too quickly to half the observed maximum and no long-time decay (thin solid curve in Figure 5). Similarly, the τ_x = 200 s

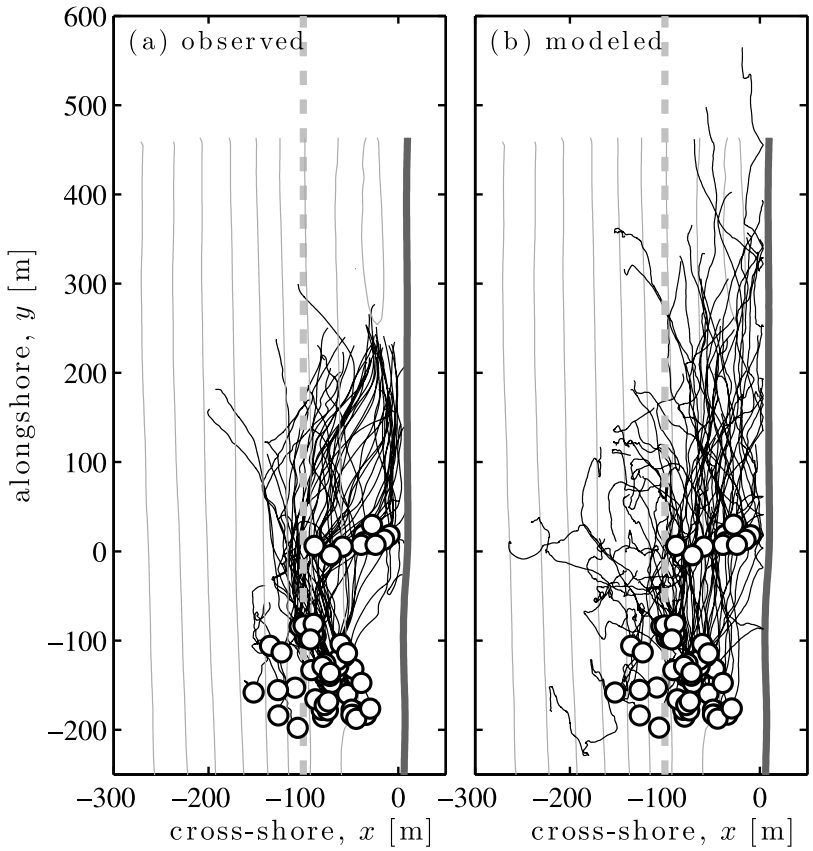

Figure 4. The (a) observed and (b) LSM modeled drifter trajectories (thin black curves) on 17 September with (τ_x, τ_y) = (125, 95) s. Open white circles are drifter release locations, and the thick gray curve near x = 0 m is the approximate shoreline. The dashed gray line indicates the outer edge of the surf zone (L_{sz} in Table 1). Bathymetry contours (thin gray) are shown at 1 m intervals.

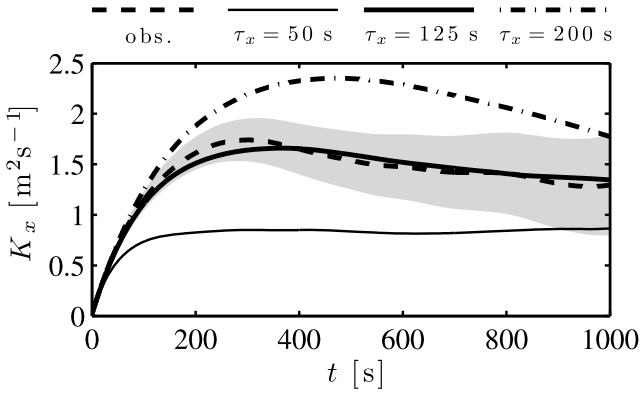

Figure 5. The observed (dashed) and LSM modeled cross-shore diffusivity K_x versus time t for release day 17 September for $\tau_x = (50, 125, 200)$ s (see legend). The gray shading indicates the observed sampling error [*Spydellet al.*, 2009].

modeled $K_x^{(m)}$ overshoots the observations, with a 50% larger maximum occurring 50% later than observed and decaying more rapidly at long times (dash-dotted curve in Figure 5).

[33] On each release day, the best fit cross-shore Lagrangian time scale τ_x is chosen to minimize the squared difference between the modeled and observed bulk diffusivity $s^2(\tau_x)$, i.e.,

$$s^2_{K_x}(\tau_x) = \frac{1}{t_{\max}} \int_0^{t_{\max}} \left[K_x^{(o)}(t) - K_x^{(m)}(t;\tau_x) \right]^2 dt, \qquad (20)$$

where $t_{\max} = 1000$ s. For each release day, the Langevin equation model (4) is run for various τ_x spanning 30–300 s (section 3.3). For all release days, the best fit τ_x varies between 75 and 200 s (Table 2), qualitatively consistent with the 116–190 s observed cross-shore diffusivity time scale [*Spydell et al.*, 2009] and consistent with the Eulerian time scale (inverse frequency) of surf zone eddies [*Feddersen et al.*, 2011]. Qualitative (nonstatistical) τ_x "error bars" are defined as the τ_x that increases s_{K_x} by 20% of $\langle (K_x^{(o)})^2 \rangle^{1/2}$, where angle brackets represent a time average over 1000 s. The τ_x error bars range between 16 and 69 s on the five release days (Table 2). The best fit τ_y (and error bars) are found by running the model with the best fit τ_x and over a 30–300 s τ_y range and minimizing the mean square error $s_{K_y}{}^2(\tau_y)$ defined analogous to (20). The resulting τ_y ranges between 95 and 155 s, similar to the best fit τ_x range (Table 3) with τ_y error bars about twice the τ_x error bars.

4. Results

[34] In this section, bulk cross-shore and alongshore diffusivities from the HB06 observations $K^{(o)}$, LSM modeled $K^{(m)}$, and analytic solution $K^{(a)}$ are compared. The analytic diffusivity $K_x^{(a)}(t)$ (see section 3.2.2) is calculated on each release day using σ_u^2 defined in (19), the best fit τ_x, and the daily pdf of cross-shore drifter initial release locations $p_0(x_0)$.

4.1. Cross-Shore Diffusivity K_x

[35] For all release days (except 14 October), the modeled $K_x^{(m)}$ and the analytic $K_x^{(a)}$ reproduce the observed $K_x^{(o)}$ (Figure 6) with small root-mean-square errors (RMSE) and high skill (Table 2) using the best fit τ_x. The modeled cross-shore diffusivity time dependence is due to the shoreline and strongly suggests that the nonmonotonic $K_x^{(o)}(t)$ is also due to the shoreline. Focusing on 17 September, the model $K_x^{(m)}$ accurately reproduces the ballistic regime ($t < 50$ s), the $K_x^{(o)}$ maximum at $t \approx 310$ s, and the slow $K_x^{(o)}$ decrease for longer t (Figure 6a). For all release days, $K_x^{(m)}$ and $K_x^{(a)}$ reproduce well $K_x^{(o)}$ (compare the dashed, solid, and dash-dotted curves in Figure 6, left) the short-time ($t < 50$ s and $t/\tau_x < 0.7$) ballistic regime $K_x = \sigma_u^2 t$. With the exception of 14 October, the modeled $K_x^{(m)}$ reproduces the observed $K_x^{(o)}$ at longer times ($t > 400$ s or $t/\tau_x > 3$, Figures 6 (left) and 6 (right), respectively). Similarly, at longer times, the analytic $K_x^{(a)}$ also reproduces $K_x^{(o)}$ on 2 and 3 October but somewhat underpredicts $K_x^{(o)}$ on 17 September and 15 October with slightly smaller skills. At intermediate times, there is variation in how well the model and analytic K_x represent the observed $K_x^{(o)}$. On 17 September and 15 October, the modeled $K_x^{(m)}$ reproduces well the magnitude and timing of the maximum $K_x^{(o)}$ (Figures 6a and 6e) whereas $K_x^{(a)}$ is generally smaller for $t > 200$ s or $t/\tau_x > 1.5$. On 2 and 3 October, the modeled and analytic K_x underpredict the $K_x^{(o)}$ maximum by approximately 1/3 but reproduce the timing of the maximum (Figures 6b and 6c).

[36] Although $K_x^{(m)}$ and $K_x^{(a)}$ are statistics of the same LSM (4) with identical release locations, $K_x^{(a)}$ and $K_x^{(m)}$ differ due to the differences in averaging. The observed diffusivities $K_x^{(o)}$ are generally limited to maximum times of $4\tau_x$ to $10\tau_x$ (Figure 6, right), due to the limited duration of drifter trajectories. Thus, the long-time limit of $K_x^{(a)}/\kappa_x = 1 - 2/\pi$ (dashed line on Figure 6, right) is generally not observed. The average cross-shore release location $\overline{x_0}$ varies between -38 and -73 m resulting in a bulk α between 3 and 40, indicating that the shoreline is encountered between the ballistic and Brownian regimes. The nondimensional K_x/κ_x dependence upon t/τ_x (Figure 6, right) is qualitatively similar to the point release analytic solution for $\alpha = 10$ (Figure 3).

[37] On 14 October, the model and analytic diffusivities poorly represent the observed diffusivity at both intermediate times ($t/\tau_x \approx 1$) and the rapid decay at long times (Figure 6d) with highest RMS error (0.55 m^2 s^{-1}) and the lowest skill of 0.87 (Table 2). As discussed by *Spydell et al.* [2009], at longer times drifter trajectories converged in the inner midsurf zone suggesting bathymetric control induces this long-time rapid decay.

4.2. Alongshore Diffusivity K_y

[38] On all release days, the model $K_y^{(m)}$ reproduces well the observed $K_y^{(o)}$ for the entire 1000 s (Figure 7, compare dashed and solid curves) with small RMS errors and high skill (>0.99, Table 3). For all times (≤1000 s), the model $K_y^{(m)}$ is within the observed $K_y^{(o)}$ uncertainty (gray shaded region in Figure 7) on all release days. The best fit τ_y (Table 3) are in the same range as the best fit τ_x (Table 2). The τ_y error bars are relatively broad indicating that a wide τ_y range would give accurate results.

[39] The relative contributions of the unbounded dispersion (i.e., the first term on right-hand side of equation (17), denoted by $K_y^{(V=0)}$) and the shear-induced K_S (the second term in equation (17)) is not understood. The shear-induced component of K_y is isolated using the $V = 0$ analytic

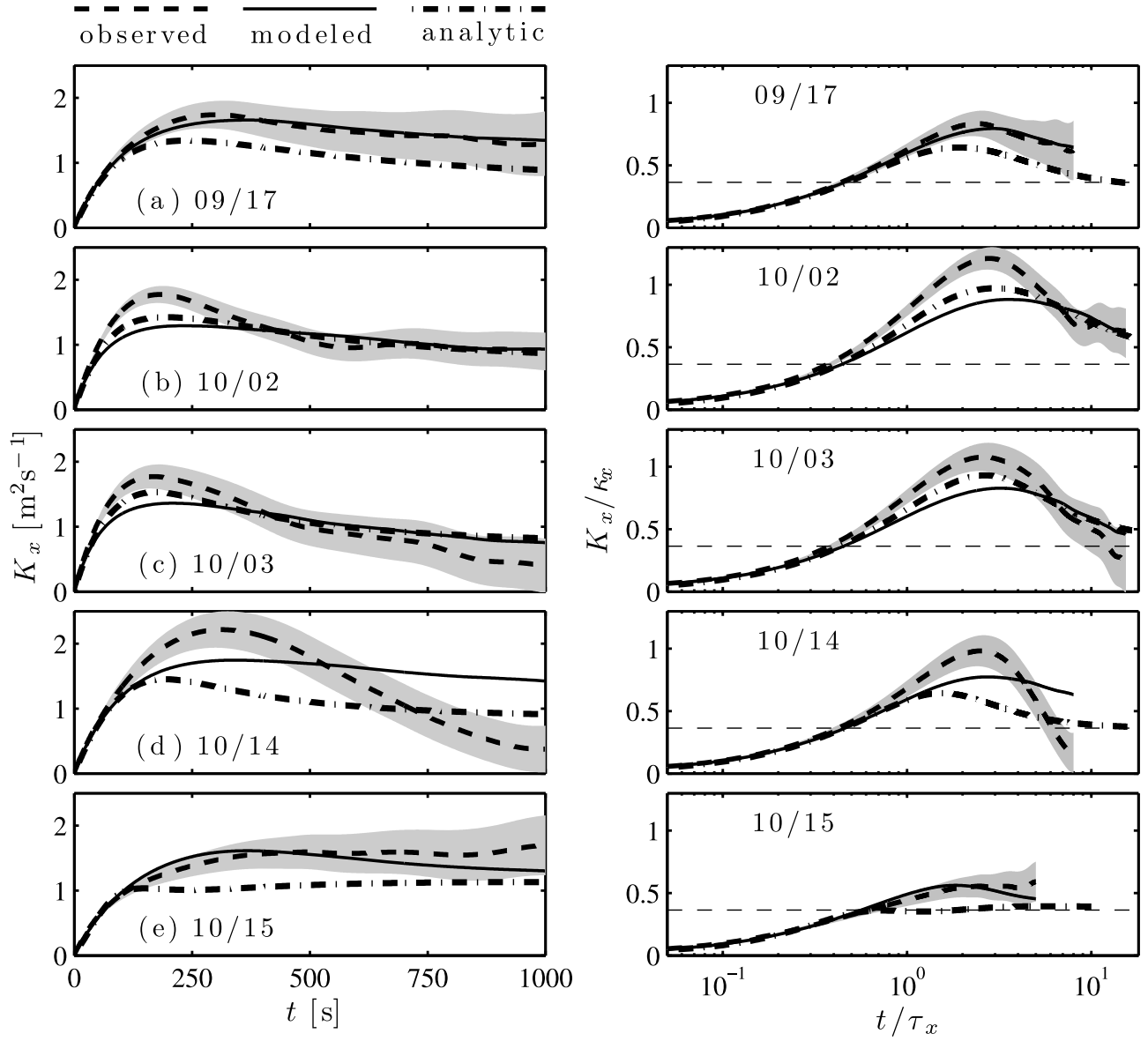

Figure 6. (left) The cross-shore diffusivity K_x versus time t and (right) the nondimensionalized diffusivity K_x/κ_x versus t/τ_x for the five HB06 release days. The observed (dashed), LSM modeled (solid), and analytic (dash-dotted) cross-shore diffusivities are shown. The shaded gray region represents the observed $K_x^{(o)}$ sampling error. For Figure 6 (right) the best fit τ_x and $\kappa_x = \sigma_u^2\tau_x$ are used to scale time and the diffusivity, respectively, and the analytic expression for the long-time $K_x/\kappa_x = (1 - 2/\pi) \approx 0.36$ is shown (thin dashed line).

unbounded diffusivity solution $K_y^{(V=0)} = \kappa_y[1 - \exp(-t/\tau_y)]$ (thin curves in Figure 7). On all release days at times $\leq \tau_y$, the $K_y^{(V=0)}$ matches $K_y^{(o)}$, indicating that at short times the diffusion is dominated by unbounded random motions (thin curves in Figure 7). On the three strong $V(x)$ release days (17 September, 14 October, and 15 October in Figure 2b), $K_y^{(V=0)}$ has a much shorter ramp-up time scale and a much smaller long-time diffusivity than $K_y^{(o)}$ (compare thin and dashed curves in Figures 7a, 7d,and 7e). In contrast, on the 2 days (2 and 3 October) with weak $V(x)$ and weak shear, the $K_y^{(V=0)}$ was only 20–30% less than the observed $K_y^{(o)}$ suggesting that shear dispersion K_S was less important than surf zone eddy-induced random dispersion.

[40] The shear-induced diffusivity K_S contribution is quantified for the observations and model by using

$$K_S^{(o,m)}(t) = K_y^{(o,m)}(t) - K_y^{(V=0)}. \quad (21)$$

The analytic shear-induced diffusivity $K_S^{(a)}$ is also calculated using (18) with the Fourier coefficients of the observed $V(x)$, the model κ_x and best fit τ_x, and the drifter-observed alongshore current L_V width (essentially 160 m, Table 4). The observed $K_y^{(o)}$, modeled $K_y^{(m)}$, and analytic diffusivities $K_S^{(a)}$ are compared in Figure 8 and Table 4.

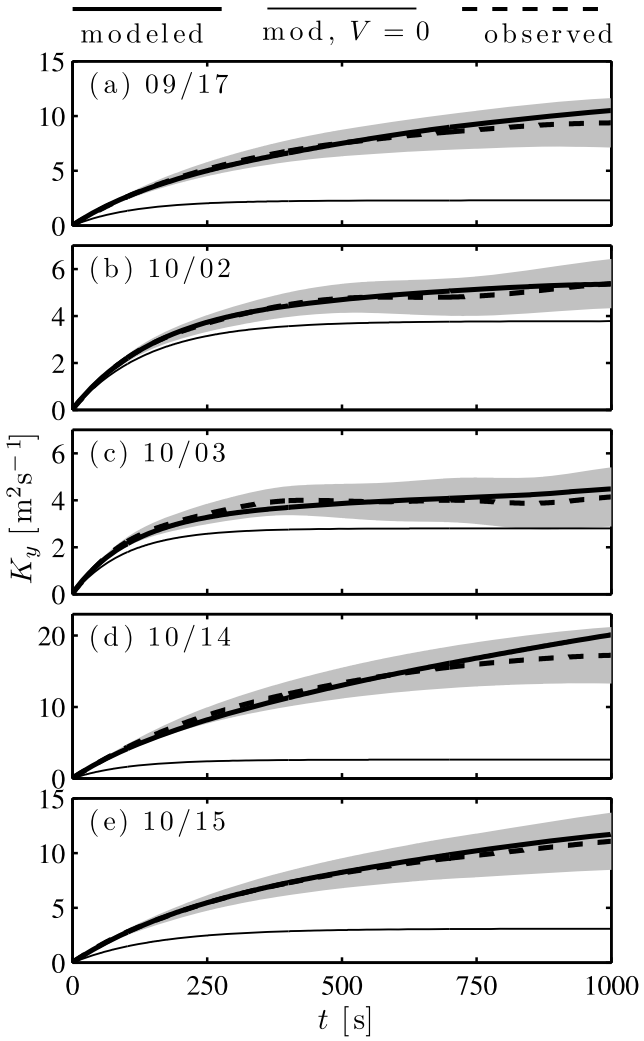

Figure 7. Alongshore diffusivity K_y versus time for the five release days. The observed (dashed), LSM modeled (thick solid) and LSM with $V = 0$ (thin solid) are indicated in the legend.

[41] The observed $K_S^{(o)}$ and modeled $K_S^{(m)}$ shear-induced diffusivity is well reproduced by the analytic $K_S^{(a)}$ on all release days (Figure 8) with high skill (≥ 0.95 except for 3 October where skill was 0.92, Table 4). The shear-dispersion-dominated release days (17 September, 14 October, and 15 October), have large K_S (>7 m^2 s^{-1}) and have a long ramp-up time scale (Figures 8a, 8d, and 8e). The difference between the observed $K_S^{(o)}$ and analytic $K_S^{(a)}$ is within the uncertainty of the observed $K_y^{(o)}$ (gray shaded region in Figure 7). This indicates that the analytic solution of *Spydell and Feddersen* [2012] for uniformly distributed cross-shore release is applicable for both low and strong current shear.

[42] For the strong $V(x)$ release days, the alongshore diffusivity K_y is dominated by shear dispersion. Consistent with this, LSM simulations with the observed $V(x)$ and small $\tau_y = 10$ s yield $K_y^{(m)}$ that are similar to $K_y^{(o)}$ (not shown) with relatively small errors and high skill (>0.91). Even on the weak $V(x)$ release days (2 and 3 October) the shear-induced K_S is greater than or equal to the cross-shore diffusivity $K_x^{(o)}$ (Figures 6b, left, and 6c, left), indicating that for alongshore uniform beaches, shear-induced dispersion is as, or more important than, cross-shore dispersion (i.e., K_x) in surf zone drifter or tracer dispersion (and thereby dilution).

5. Discussion

5.1. Cross-Shore Diffusivity

[43] A Lagrangian stochastic model, that includes the shoreline and has cross-shore uniform velocity variance σ_u^2 and Lagrangian time scale τ_x, reproduces the first 1000 s of the nonmonotonic observed cross-shore diffusivity $K_x^{(o)}$ (Figure 6). This includes the ballistic regime, the magnitude and timing of the $K_x^{(o)}$ maxima, and the longer time decay. On 3 of the 5 days the cross-shore diffusivity maximum is under predicted by about 30% and may be due to the use of cross-shore constant velocity variance and Lagrangian time scale when they are cross-shore dependent. The modeled and analytic $K_x^{(m,a)}$ maximum and longer-time decay is due to the presence of the shoreline strongly suggesting that the observed nonmonotonic $K_x^{(o)}$ is also due to the shoreline. The hypothesis that diffusivity is weaker seaward of the surf zone (either by smaller $\overline{u^2}$ or τ_x) is not necessary to explain the first 1000 s of the observed K_x time dependence. The model has high skill with bulk cross-shore uniform σ_u^2 and τ_x, even though the observed cross-shore velocity variance $\overline{u^2}$ is clearly cross-shore dependent (Figure 2c) and the cross-shore dependence of τ_x is not known. This suggests that, for at least the first 1000 s, the effect of cross-shore variable statistics is weak.

[44] Assuming that a region of reduced diffusivity seaward of the surf zone exists (i.e., $\kappa_x^{(sea)} < \kappa_x^{(surf)}$), then the diffusive time $\tau_D = L^2/\kappa_x$ (where L is the cross-shore length scale of the surf zone) required for surf zone released particles to begin to "feel" the reduced diffusivity is ~10,000 s (Table 4), much longer than the 1000 s of observed dispersion. At times greater than τ_D, the bulk drifter-derived cross-shore diffusivity would be reduced by the lower seaward of the surf zone diffusivity region and approach $(1 - 2/\pi)\kappa_x^{(sea)}$, where the factor $(1 - 2/\pi)$ is due to the shoreline. If horizontal diffusion is significantly weaker seaward of the surf zone, the HB06 drifter tracks were too short to observe it.

[45] For the modeled and analytic cross-shore diffusivities, particles are reflected at the shoreline resulting in a no flux boundary condition. However, the GPS-tracked drifters did not follow this boundary condition. Drifters that came too close to the shoreline and were grounded (or "beached") had their trajectories terminated and were rereleased

Table 4. Alongshore Shear-Induced Diffusivity K_S Parameters and Model Errors and Skills for the Five HB06 Drifter Release Days[a]

	17 Sep	2 Oct	3 Oct	14 Oct	15 Oct
L_V (m)	150	167	169	150	151
$K_S^{(a)}$ RMSE (m^2 s^{-1})	0.40	0.09	0.28	2.28	0.54
$K_S^{(a)}$ skill	0.99	0.99	0.92	0.95	0.99
$\tau_D(\times 10^4)$ (s)	1.07	1.65	1.50	1.00	0.80
τ_x/τ_D	0.012	0.005	0.005	0.013	0.025

[a]The cross-shore extent of the alongshore current is given as L_V. The K_S RMSE is defined as $\langle (K_S^{(a)} - K_S^{(o)})^2 \rangle$ and skill is defined as in Table 2. The ratio τ_x/τ_D is calculated with the parameters in Table 2 and $\tau_D = L_V^2/\kappa_x$.

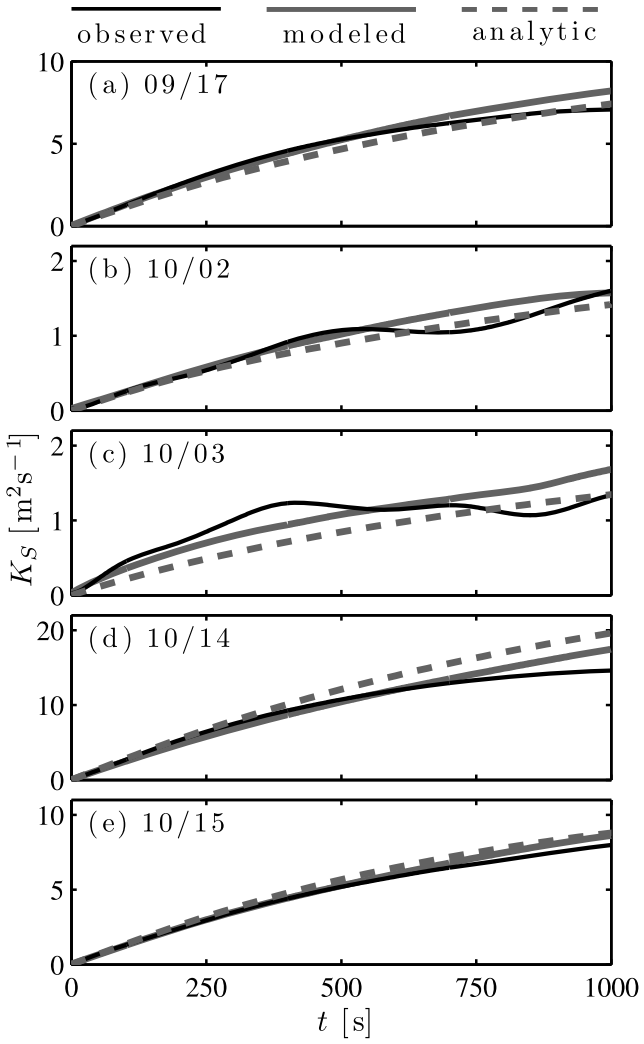

Figure 8. The shear-induced observed $K_S^{(o)}$ (thin solid curve), LSM modeled $K_S^{(m)}$ (thick solid curve), and analytic $K_S^{(a)}$ (equation (18), dashed curve) alongshore diffusivity versus time for each release day.

further offshore. Thus, the boundary condition for the observed drifters is mixed: some drifters reflected off the shoreline while others (the ones which grounded) were absorbed. Repeating the analysis that led to (15), but with an absorbing (rather than no flux) boundary condition, results in an analytic cross-shore diffusivity similar to the no-flux $K_x^{(a)}$. For $\alpha \approx 10$ (the order of magnitude here, Table 2), the absorbing diffusivity also has a distinct maximum and at long-time approaches a constant $\kappa_x(2 - \pi/2) = 0.43\kappa_x$ which is only slightly larger than the no-flux constant $\kappa_x(1 - 2/\pi) = 0.36\kappa_x$.

5.2. Alongshore Diffusivity

[46] The analytic shear-induced diffusivity $K_S^{(a)}$ accurately reproduces the observed shear-induced alongshore dispersion (Figure 8) for both strong and weak alongshore current shear release days. Although the observed drifter position pdf is not uniform and varies from day to day (Figure 2a), the cross-shore uniform drifter distribution assumption used in (18) does not affect the results. *Spydell et al.* [2009] found the alongshore diffusive time scale T_y by (essentially) fitting the observed alongshore diffusivity $K_y^{(o)}(t)$ to $\kappa_y[1 - \exp(-t/T_y)]$. For the 3 days with strong shear dispersion (17 September, 14 October, and 15 October) this T_y varied between 340 and 420 s [*Spydell et al.*, 2009, Table 1], significantly larger than the best fit Lagrangian time scale τ_y found here (Table 3). In contrast, when shear dispersion was weak and the alongshore diffusivity was dominated by unbounded random dispersion (2 and 3 October), the *Spydell et al.* [2009] Lagrangian time scale $T_y = (190, 118)$ s is consistent with the best fit $\tau_y = (140, 100)$ s here.

[47] Given the L_V, κ_x, and τ_x parameters for the strong $V(x)$ days (see Tables 2 and 4), $\tau_D = L_V^2/\kappa_x$ varies between 8000 and 10,700 s and τ_x/τ_D varies between 0.012 and 0.025 (Table 4). For $\tau_x/\tau_D \approx 0.01$, the shear dispersion $K_S^{(a)}(t)$ time dependence straddles the very small τ_x ($\ll \tau_D$) exponential ($\propto 1 - \exp(-\pi^2 t/\tau_D)$), and the moderate τ_x error function ($\propto \mathrm{erf}(t/\tau_S)$, where $\tau_S = (2\tau_x\tau_D)^{1/2}/\pi$ is the appropriate shear dispersion time scale [*Spydell and Feddersen*, 2012]) time dependence. Although $K_S^{(a)}(t)$ is neither of these functions, the time scale τ_S varies between 480 and 580 s over all release days, consistent with the ramp-up time for the observed, modeled, and analytic $K_S(t)$ (Figure 8). Moreover, on the three strong $V(x)$ release days, τ_S is also qualitatively consistent with the observed *Spydell et al.* [2009] $K_y^{(o)}(t)$ time scale T_y (340–420 s) that combines random unbounded dispersion and shear dispersion. This further demonstrates the consistency of the nonzero τ_x shear dispersion theory and also demonstrates that the ramp-up time scale of the alongshore diffusivity cannot be interpreted as a Lagrangian time scale.

[48] The reason *Spydell et al.* [2009] inferred a factor of 3 difference from shear dispersion theory was because a parabolic $V(x)$ profile was used in order to directly apply the classic *Taylor* [1953] theory for laminar $\tau_x = 0$ shear dispersion. Furthermore, the shear dispersion theory of *Spydell and Feddersen* [2012], used here to estimate $K_S^{(a)}$, is applicable for any Lagrangian time scale $\tau_x \geq 0$. For the values of τ_x/τ_D observed on the strong $V(x)$ release days (0.012–0.025, Table 4), the classic Taylor theory using the observed $V(x)$ yields shear-induced diffusivities that are 10–20% smaller than the $K_S^{(a)}$ calculated here. Thus, the *Taylor* [1953] theory can underpredict shear-induced dispersion in the surf zone or in other turbulent flows where the cross-domain Lagrangian time scale is sufficiently large.

5.3. Qualitatively Simulating Pollution Dispersal: LSM Model Parameters

[49] Complex wave-resolving or wave-averaged surf zone wave and circulation models with a coupled tracer or drifter model can be used to simulate the transport and dispersal of a beach (shoreline) pollution spill. Such models have been used to reproduce surf zone observed drifter dispersion [*Spydell and Feddersen*, 2009; *Reniers et al.*, 2009] and surf zone observed dye tracer transport and dispersion [*Clark et al.*, 2011]. Such models contain the detailed physics of surf zone eddy-induced stirring [e.g., *Spydell and Feddersen*, 2009; *Long and Özkan-Haller*, 2009; *Reniers et al.*, 2009] that induces horizontal dispersion of drifters and tracer [*Spydell et al.*, 2007; *Spydell and Feddersen*, 2009; *Clark et al.*, 2010, 2011; *Geiman et al.*, 2011]. However, the complexity of these models also can be prohibitive in

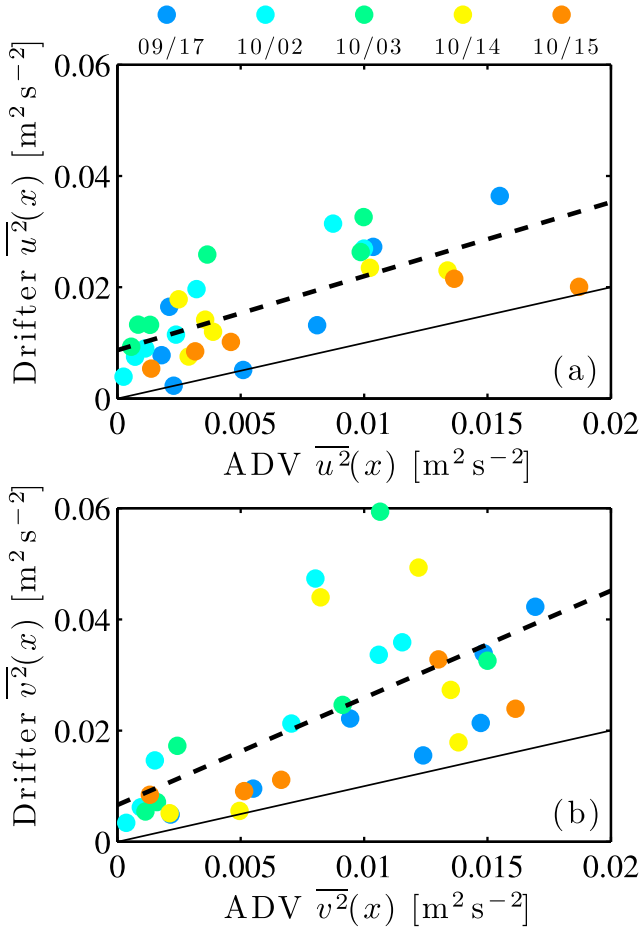

Figure 9. Drifter-derived versus ADV-derived (a) $\overline{u^2}(x)$ and (b) $\overline{v^2}(x)$. The drifter velocity variances are interpolated to the ADV locations. The thin black line represents the 1:1 relationship, and the dashed black line represents the best fit line. In Figure 9a the best fit slope m = 1.3, intercept b = 0.009, and correlation r = 0.72, and in Figure 9b the best fit slope m = 1.9, b = 0.007, and correlation r = 0.67.

terms of setting them up and running them sufficiently rapidly to provide useful qualitative estimates of surf zone pollution dispersal.

[50] Given the model parameters $V(x)$, σ_u^2, σ_v^2, τ_x, and τ_y, the LSM model can be used both numerically and analytically to predict well at least the first 1000 s of the transport and dispersion of pollution (e.g., shoreline contaminant spill). Here, the model parameters are derived from the drifter observations. However, in general LSM model parameters need to be a priori specified to simulate pollution dispersion. These parameters can be approximately estimated with varying levels of uncertainty from relatively simple models (e.g., $V(x)$), empirical relationships (e.g., σ_u^2), and from knowledge of surf zone eddy Eulerian time scales (τ_x, and τ_y).

[51] Shear dispersion is often the most significant component to the overall diffusivity, particularly for significant alongshore current shear (as on 17 September, 14 October, and 15 October). Thus, resolving the mean alongshore current $V(x)$ is critical. Both very simple one-dimensional alongshore current models [e.g., *Ruessink et al.*, 2001] or more complex wave-averaged [e.g., *Shi et al.*, 2011] or wave-resolving [e.g., *Chen et al.*, 2003; *Feddersen et al.*, 2011] models have been shown to model $V(x)$ well given the bathymetry and incident wavefield.

[52] The bulk (cross-shore averaged) low-frequency ($f < 0.03$ Hz) Lagrangian velocity variances σ_u^2 and σ_v^2 are derived from the low-frequency quasi-Eulerian cross-shore-dependent $\overline{u^2}(x)$ and $\overline{v^2}(x)$. For velocities which include sea swell motions as well as low-frequency ones, quasi-Eulerian binned drifter velocity variances are similar to ADV-measured Eulerian velocity variances [see *Spydell et al.*, 2009, Figures 2b and 2c]. Similarly, the low-frequency drifter-derived $\overline{u^2}(x)$ and $\overline{v^2}(x)$ are correlated with (r = 0.72 and r = 0.67) but are roughly 1.3 and 1.9, respectively, times larger than ADV-measured low-frequency velocity variances (Figure 9). An Eulerian bulk rotational velocity variance [*Lippmann et al.*, 1999] that removes the infragravity wave component but combines cross-shore and alongshore velocities is similar to the Eulerian low-frequency velocity variance (not shown). Thus, at low frequencies, infragravity wave motions, which do not lead to diffusion, are weak relative to rotational velocities. The relationship between the binned drifter and ADV-measured velocity variances (Figure 9) implies that knowledge of the Eulerian low-frequency (<0.03 Hz) velocity variance can be used to approximately estimate the σ_u^2 and σ_v^2, albeit with substantial uncertainty.

[53] Without in situ observations, the Eulerian low-frequency velocity variance must still be specified. Although the Eulerian low-frequency velocities can be reasonably well modeled with a complex surf zone circulation model [*Reniers et al.*, 2007; *Feddersen et al.*, 2011], running such a model goes against the idea of using a simple LSM. Eulerian rotational velocities (responsible for the dispersion) are driven by both shear instabilities [*Allen et al.*, 1996] and wave breaking of a directionally spread wavefield [*Peregrine*, 1998; *Spydell and Feddersen*, 2009]. Although the contribution of each driver is not well understood, bulk (low-frequency) rotational velocities are approximately linearly related to the local mean alongshore current magnitude $|V|$ [see *Noyes et al.*, 2004, Figure 8; see also of *Feddersen et al.*, 2011, Figures 14 and 15]. The bulk rotational velocities are roughly evenly split between $\overline{u^2}$ and $\overline{v^2}$ [e.g., *Noyes et al.*, 2004], except near the shoreline where $\overline{v^2}$ dominates [*Feddersen et al.*, 2011]. These observations can provide a simple way to approximately parameterize σ_u^2 and σ_v^2 using $V(x)$.

[54] The Lagrangian time scale remains to be specified, and has the largest uncertainty in a priori specification. Here, the best fit τ_x ranged between 75 and 200 s, and observed drifter-derived $K_x^{(o)}$ ramp-up times are always less than 200 s [*Spydell et al.*, 2007, 2009; *Brown et al.*, 2009]. The best fit Lagrangian time scale τ_x is not correlated with other potential time scales (e.g., peak wave period or L/σ_u) nor wave/current conditions (e.g., H_s or V). However, the variation of these parameters may have been too small to observe any such potential relationship.

[55] The relationship between Eulerian (τ_E) and Lagrangian time scales in the surf zone is not understood. However, in the open ocean the ratio of Lagrangian to Eulerian τ generally ranges between 0.5 and 1.25 [e.g.,

Lumpkin et al., 2002]. Using the Lagrangian time scale range of τ found here and inferred Eulerian time scales of surf zone eddies [e.g., *Noyes et al.*, 2004; *Spydell and Feddersen*, 2009; *Long and Özkan-Haller*, 2009], the ratio τ/τ_E in the surf zone is similar to the open ocean observations. Generally, weaker $V(x)$ release days have significantly (relative to the error bars) smaller best fit τ_x = 75 s than stronger $V(x)$ release days with $\tau_x \geq 125$ s (Table 2). This may reflect reduced longer-time scale shear instability-induced eddies and increased shorter time scale directionally spread breaking wave generated eddies relative to stronger $V(x)$ release days. The best fit τ_x and τ_y are generally similar (Tables 2 and 3) and for strong $V(x)$, where shear-induced alongshore dispersion dominates, varying τ_y has a small effect on K_y at longer times. Therefore, although significant uncertainty remains, setting τ_x = 75 s for weak $V(x)$ and larger τ_x ($\approx$ 150 s) for stronger $V(x)$, together with $\tau_y = \tau_x$, may give qualitatively reasonable diffusivity estimates. One benefit of the analytic solutions, is that the K variation induced by varying the Lagrangian time scale can be readily evaluated.

6. Summary

[56] The observed cross-shore (K_x) and alongshore (K_y) diffusivities for five release days on an alongshore uniform beach were reproduced by Lagrangian stochastic model (LSM) simulations and analytic solutions. The model solves for particle trajectories using the observed bulk Lagrangian velocity variance and alongshore current. The best fit cross-shore and alongshore Lagrangian time scales, found by minimizing the difference between the modeled and observed diffusivities, generally range between 75 and 200 s, and are consistent with the Eulerian time scale (inverse frequency) of surf zone eddies. Although velocity variances are considerably cross-shore dependent, the model works well assuming homogeneous velocity variances and Lagrangian time scales.

[57] The features of the time-dependent observed K_x, initial ballistic growth to a maximum and slow long-time decay, are explained by the presence of a shoreline boundary. Weaker diffusivity seaward of the surf zone is not required to explain the observed K_x features over 1000 s. The observed drifter trajectories were too short to observe the analytic long-time limit for K_x or to deduce whether the seaward of the surf zone diffusivity is weaker than within the surf zone.

[58] The alongshore diffusivity K_y has two components: a random unbounded dispersion component due to surf zone eddies and a shear dispersion component K_S induced by cross-shore shear in the alongshore current $V(x)$. On release days with moderate-to-strong $V(x)$, the alongshore diffusivity was dominated by shear dispersion K_S. Even on weak $V(x)$ release days where shear dispersion K_S is about 1/3 of K_y, shear dispersion K_S is approximately the same magnitude of the cross-shore diffusivity K_x. The analytic K_S, which assumes cross-shore uniformly distributed drifters and includes the effects of nonzero Lagrangian time scale, accurately reproduces the inferred shear dispersion on all release days (both strong and weak $V(x)$). Although not in the correct asymptotic regime, an approximate analytic time scale is qualitatively consistent with the observed K_S time scale.

[59] With a priori knowledge of the bathymetry and incident wavefield, the alongshore current $V(x)$ can be accurately predicted, and can be used to parameterize the Lagrangian stochastic model inputs, allowing for simple predictions of the dispersal of an initial value problem of a beach contaminant spill.

[60] **Acknowledgments.** This analysis was supported by NSF, ONR, and CA Sea Grant. The HB06 field work was supported by CA Coastal Conservancy, NOAA, NSF, ONR, and CA Sea Grant. R. T. Guza was a co-PI on the HB06 experiment. Staff and students from the Integrative Oceanography Division (B. Woodward, B. Boyd, K. Smith, D. Darnell, I. Nagy, D. Clark, M. Omand, M. Yates, M. McKenna, M. Rippy, S. Henderson) were instrumental in acquiring the field observations.

References

Allen, J. S., P. A. Newberger, and R. A. Holman (1996), Nonlinear shear instabilities of alongshore currents on plane beaches, *J. Fluid Mech.*, *310*, 181–213, doi:10.1017/S0022112096001772.

Berloff, P. S., and J. C. McWilliams (2002), Material transport in oceanic gyres. Part II: Hierarchy of stochastic models, *J. Phys. Oceanogr.*, *32*(3), 797–830.

Boehm, A. B., S. B. Grant, J. H. Kim, C. D. McGee, S. Mowbray, C. Clark, D. Foley, and D. Wellmann (2002), Decadal and shorter period variability of surf zone water quality at Huntington Beach, California, *Environ. Sci. Technol.*, *36*, 3885–3892, doi:10.1021/es020524u.

Brickman, D., and P. C. Smith (2002), Lagrangian stochastic modeling in coastal oceanography, *J. Atmos. Oceanic Technol.*, *19*(1), 83–99.

Brown, A., and A. McLachlan (2002), Sandy shore ecosystems and the threats facing them: Some predictions for the year 2025, *Environ. Conserv.*, *29*, 62–77.

Brown, J., J. MacMahan, A. Reniers, and E. Thornton (2009), Surf zone diffusivity on a rip-channeled beach, *J. Geophys. Res.*, *114*, C11015, doi:10.1029/2008JC005158.

Chen, Q., J. T. Kirby, R. A. Dalrymple, F. Shi, and E. B. Thornton (2003), Boussinesq modeling of longshore currents, *J. Geophys. Res.*, *108*(C11), 3362, doi:10.1029/2002JC001308.

Clark, D. B., F. Feddersen, and R. T. Guza (2010), Cross-shore surfzone tracer dispersion in an alongshore current, *J. Geophys. Res.*, *115*, C10035, doi:10.1029/2009JC005683.

Clark, D. B., F. Feddersen, and R. T. Guza (2011), Modeling surf zone tracer plumes: 2. Transport and dispersion, *J. Geophys. Res.*, *116*, C11028, doi:10.1029/2011JC007211.

Davis, R. E. (1991), Observing the general circulation with floats, *Deep Sea Res.*, *38*, S531–S571.

Feddersen, F. (2012), Observations of the surfzone turbulent dissipation rate, *J. Phys. Oceanogr.*, doi:10.1175/JPO-D-11-082.1, in press.

Feddersen, F., D. B. Clark, and R. T. Guza (2011), Modeling surf zone tracer plumes: 1. Waves, mean currents, and low-frequency eddies, *J. Geophys. Res.*, *116*, C11027, doi:10.1029/2011JC007210.

Geiman, J. D., J. T. Kirby, A. J. H. M. Reniers, and J. H. MacMahan (2011), Effects of wave averaging on estimates of fluid mixing in the surf zone, *J. Geophys. Res.*, *116*, C04006, doi:10.1029/2010JC006678.

Grant, S. B., J. H. Kim, B. H. Jones, S. A. Jenkins, J. Wasyl, and C. Cudaback (2005), Surf zone entrainment, along-shore transport, and human health implications of pollution from tidal outlets, *J. Geophys. Res.*, *110*, C10025, doi:10.1029/2004JC002401.

Haile, R. W., et al. (1999), The health effects of swimming in ocean water contaminated by storm drain runoff, *Epidemiology*, *10*, 355–363.

Jiang, S. C., and W. Chu (2004), PCR detection of pathogenic viruses in southern California urban rivers, *J. Appl. Microbiol.*, *97*, 17–28.

Lippmann, T. C., T. H. C. Herbers, and E. B. Thornton (1999), Gravity and shear wave contributions to nearshore infragravity motions, *J. Phys. Oceanogr.*, *29*(2), 231–239.

Long, J. W., and H. T. Özkan-Haller (2009), Low-frequency characteristics of wave group-forced vortices, *J. Geophys. Res.*, *114*, C08004, doi:10.1029/2008JC004894.

Lumpkin, R., A. Treguier, and K. Speer (2002), Lagrangian eddy scales in the northern Atlantic Ocean, *J. Phys. Oceanogr.*, *32*(9), 2425–2440.

Middleton, J. F. (1985), Drifter spectra and diffusivities, *J. Mar. Res.*, *43*(1), 37–55.

Noyes, T. J., R. T. Guza, S. Elgar, and T. H. C. Herbers (2004), Field observations of shear waves in the surf zone, *J. Geophys. Res.*, *109*, C01031, doi:10.1029/2002JC001761.

Pasquero, C., A. Provenzale, and A. Babiano (2001), Parameterization of dispersion in two-dimensional turbulence, *J. Fluid Mech.*, *439*, 279–303, doi:10.1017/S0022112001004499.

Peregrine, D. H. (1998), Surf zone currents, *Theor. Comput. Fluid Dyn.*, *10*, 295–309.

Reeves, R. L., S. B. Grant, R. D. Mrse, C. M. C. Oancea, B. F. Sanders, and A. B. Boehm (2004), Scaling and management of fecal indicator bacteria in runoff from a coastal urban watershed in southern California, *Environ. Sci. Technol.*, *38*, 2637–2648.

Reniers, A. J. H. M., J. H. MacMahan, E. B. Thornton, and T. P. Stanton (2007), Modeling of very low frequency motions during RIPEX, *J. Geophys. Res.*, *112*, C07013, doi:10.1029/2005JC003122.

Reniers, A. J. H. M., J. H. MacMahan, E. B. Thornton, T. P. Stanton, M. Henriquez, J. W. Brown, J. A. Brown, and E. Gallagher (2009), Surf zone surface retention on a rip-channeled beach, *J. Geophys. Res.*, *114*, C10010, doi:10.1029/2008JC005153.

Rodean, H. C. (1996), *Stochastic Lagrangian Models of Turbulent Diffusion, Meteorol. Monogr. Ser.*, vol. 48, Am. Meteorol. Soc., Boston, Mass.

Ruessink, B. G., J. R. Miles, F. Feddersen, R. T. Guza, and S. Elgar (2001), Modeling the alongshore current on barred beaches, *J. Geophys. Res.*, *106*, 22,451–22,463, doi:10.1029/2000JC000766.

Schmidt, W. E., B. T. Woodward, K. S. Millikan, R. T. Guza, B. Raubenheimer, and S. Elgar (2003), A GPS-tracked surf zone drifter, *J. Atmos. Oceanic Technol.*, *20*(7), 1069–1075.

Shi, F., D. M. Hanes, J. T. Kirby, L. Erikson, P. Barnard, and J. Eshleman (2011), Pressure-gradient-driven nearshore circulation on a beach influenced by a large inlet-tidal shoal system, *J. Geophys. Res.*, *116*, C04020, doi:10.1029/2010JC006788.

Siegel, D. A., B. P. Kinlan, B. Gylord, and S. D. Gaines (2003), Lagrangian descriptions of marine larval dispersion, *Mar. Ecol. Prog. Ser.*, *260*, 83–96.

Spydell, M. S., and F. Feddersen (2009), Lagrangian drifter dispersion in the surf zone: Directionally spread, normally incident waves, *J. Phys. Oceanogr.*, *39*, 809–830.

Spydell, M. S., and F. Feddersen (2012), The effect of a non-zero Lagrangian time-scale on bounded shear dispersion, *J. Fluid Mech.*, *691*, 69–94, doi:10.1017/jfm.2011.443.

Spydell, M., F. Feddersen, R. T. Guza, and W. E. Schmidt (2007), Observing surf-zone dispersion with drifters, *J. Phys. Oceanogr.*, *37*, 2920–2939.

Spydell, M. S., F. Feddersen, and R. T. Guza (2009), Observations of drifter dispersion in the surf zone: The effect of sheared alongshore currents, *J. Geophys. Res.*, *114*, C07028, doi:10.1029/2009JC005328.

Taylor, G. I. (1922), Diffusion by continuous movements, *Proc. London Math. Soc.*, *20*, 196–212.

Taylor, G. I. (1953), Dispersion of soluble matter in solvent flowing slowly through a tube, *Proc. R. Soc. London, Ser. A*, *219*, 186–203.

Uhlenbeck, G. E., and L. S. Ornstein (1930), On the theory of the Brownian motion, *Phys. Rev.*, *36*, 823–841.

Wilson, J., and B. Sawford (1996), Review of Lagrangian stochastic models for trajectories in the turbulent atmosphere, *Boundary Layer Meteorol.*, *78*(1), 191–210.

Wilson, J. D., T. K. Flesch, and G. E. Swaters (2003), Dispersion in sheared Gaussian homogeneous turbulence, *Boundary Layer Meteorol.*, *62*, 281–290.

Zambianchi, E., and A. Griffa (1994), Effects of finite scales of turbulence on dispersion estimates, *J. Mar. Res.*, *52*, 129–148.

F. Feddersen and M. S. Spydell, Integrative Oceanography Division, Scripps Institution of Oceanography, University of California, San Diego, 9500 Gilman Dr., La Jolla, CA 92093-0209, USA. (falk@coast.ucsd.edu; mspydell@ucsd.edu)